Simple replication methods for producing nanoslits in thermoplastics and the transport dynamics of double-stranded DNA through these slits†

Rattikan Chantiwas,[abe] Mateusz L. Hupert,[ab] Swathi R. Pullagurla,[a] Subramanian Balamurugan,[a] Jesús Tamarit-López,[f] Sunggook Park,[bc] Proyag Datta,[d] Jost Goettert,[d] Yoon-Kyoung Cho[e] and Steven A. Soper*[abce]

Received 12th June 2010, Accepted 9th September 2010
DOI: 10.1039/c0lc00096e

Mixed-scale nano- and microfluidic networks were fabricated in thermoplastics using simple and robust methods that did not require the use of sophisticated equipment to produce the nanostructures. High-precision micromilling (HPMM) and photolithography were used to generate mixed-scale molding tools that were subsequently used for producing fluidic networks into thermoplastics such as poly(methyl methacrylate), PMMA, cyclic olefin copolymer, COC, and polycarbonate, PC. Nanoslit arrays were imprinted into the polymer using a nanoimprinting tool, which was composed of an optical mask with patterns that were 2–7 μm in width and a depth defined by the Cr layer (100 nm), which was deposited onto glass. The device also contained a microchannel network that was hot embossed into the polymer substrate using a metal molding tool prepared *via* HPMM. The mixed-scale device could also be used as a master to produce a polymer stamp, which was made from polydimethylsiloxane, PDMS, and used to generate the mixed-scale fluidic network in a single step. Thermal fusion bonding of the cover plate to the substrate at a temperature below their respective T_g was accomplished by oxygen plasma treatment of both the substrate and cover plate, which significantly reduced thermally induced structural deformation during assembly: ~6% for PMMA and ~9% for COC nanoslits. The electrokinetic transport properties of double-stranded DNA (dsDNA) through the polymeric nanoslits (PMMA and COC) were carried out. In these polymer devices, the dsDNA demonstrated a field-dependent electrophoretic mobility with intermittent transport dynamics. DNA mobilities were found to be $8.2 \pm 0.7 \times 10^{-4}$ cm^2 V^{-1} s^{-1} and $7.6 \pm 0.6 \times 10^{-4}$ cm^2 V^{-1} s^{-1} for PMMA and COC, respectively, at a field strength of 25 V cm^{-1}. The extension factors for λ-DNA were 0.46 in PMMA and 0.53 in COC for the nanoslits (2–6% standard deviation).

Introduction

Nanofluidic vias are defined as a conduit with one dimension (nanoslit) or two dimensions (nanochannel) in the nanometre scale (1–100 nm).[1] Nanofluidic networks are beginning to find many important applications in biology and medicine because they can provide molecular-scale information that cannot be realized in micro-scale domains.[1,2] For example, because nanofluidic vias contain a size similar to the persistence length of dsDNA (~50 nm), DNAs can be sized and/or mapped directly by transporting these biopolymers through nano-scale conduits. This translocation process induces stretching to near the full contour length of the dsDNA.[2–6] Efforts are now being investigated toward developing intriguing DNA sequencing platforms using nanofluidic vias as well.[2,7–13] Protein molecular structure can also be evaluated *via* nanochannel translocation.[14,15]

Most of the biopolymer translocation work has been carried out using fused silica or quartz patterned through either wet or dry etching processes following optical lithography, which generates nanoslits.[16,17] For nanochannels, in which both the depth and width possess dimensions below 100 nm, the patterning tool required for the channel width (below the diffraction limit for optical lithography) and depth can be achieved by a focused ion beam,[18] proton beam,[19] electron beam[20] or nanoimprint lithography (NIL) followed by a subsequent pattern transfer into the underlying substrate through dry etching.[21] While these are well established techniques founded on Si-based processing, they do not lend themselves well to large-scale, low-cost production of nano-scale devices required for diagnostic applications where one-time use devices are paramount to eliminate potential problems arising from sample carry-over artifacts.[22–24]

A diverse array of techniques can be employed to make structures from the nm to μm range in thermoplastics that can

[a]*Department of Chemistry, Louisiana State University, Baton Rouge, LA, 70803, USA. E-mail: chsope@lsu.edu; Fax: +1 (225) 578-3458; Tel: +1 (225) 578-1527*
[b]*Center for Bio-Modular Multi-Scale Systems, Louisiana State University, Baton Rouge, LA, 70803, USA*
[c]*Department of Mechanical Engineering, Louisiana State University, Baton Rouge, LA, 70803, USA*
[d]*Center for Advanced Microstructures and Devices, Louisiana State University, Baton Rouge, LA, 70803, USA*
[e]*School of Nano-Bioscience and Chemical Engineering, Ulsan National Institute of Science and Technology, Ulsan, South Korea*
[f]*Departamento de Quimica, Instituto de Reconocimiento Molecular y Desarrollo Tecnologico, Universidad Politecnica de Valencia, Camino de Vera s/n, 46071 Valencia, Spain*

† Electronic supplementary information (ESI) available: Effects of nanoimprinting conditions on microchannel geometry (Fig. S1). Metrology of nanoslits after assembly (Fig. S2). XPS surface analysis data (Table S1, Fig. S3). Images showing intermittent movement of DNA through nanoslits (Fig. S4). See DOI: 10.1039/c0lc00096e

provide simple manufacturing capabilities and high production rates, such as nano-replication.[25–27] For nano-replication, a single molding tool can be used to produce large numbers of replicas without requiring to pattern structures using an ion or electron beam for each device. In addition, when employing replication techniques, the same molding tool can be used to produce replicas in a variety of materials to generate surface chemistries appropriate for the given application.[28] Due to the diverse array of surface chemistries afforded by various thermoplastics, there is a wealth of modification chemistries that can be used for these materials to further alter their surface properties.[28–32] Hence, thermoplastics are attractive substrate materials for many fluidic systems.[1,33]

As examples of nanofabrication in thermoplastics, Li *et al.* fabricated self-sealed nanofluidic conduits (100 × 100 nm^2) employing a sacrificial technique and NIL in the polymer, poly(butylnorbornene), and subsequently used this device to study electrically driven DNA translocation through the channels.[34] Guo *et al.* fabricated a Si mold by lithography and deep reactive ion etching with the pattern transferred into poly(methyl methacrylate), PMMA, to create nano-conduits (300 × 700 nm^2, 300 × 500 nm^2 and 75 × 120 nm^2). The channels were sealed using NIL instrument and DNA stretching was described.[35] Recently, Thamdrup and co-workers fabricated square PMMA channels (250 × 250 nm^2) using NIL from a Si stamp that was prepared *via* E-beam lithography and dsDNA translocation through these channels was also described.[36] Despite the use of the NIL process, all of the nanostructures in the aforementioned works were formed in a thin layer of resist spin-coated onto a Si or quartz substrate, which significantly lowers the throughput of the fabrication process and as a result makes it difficult to realize the production of low-cost nanofluidic devices.

In this work, we report simple and novel fabrication techniques for generating devices in bulk thermoplastic polymers containing mixed-scale structures (microstructures and nanoslits) using replication-based technologies. The process reported here consists of using a metal molding tool prepared *via* high-precision micromilling (HPMM) to generate microfluidic channels by hot embossing into a polymer substrate. The nanofluidic vias were prepared using nanoimprinting of the microstructured substrate with an optical mask. The optical mask consisted of a sodalime glass plate with a thin Cr layer (~100 nm, defined the nanoslit depth) that was patterned using standard optical lithography to make stripes that were 2–7 μm in width. The imprinting was performed by clamping the substrate containing the microstructures between a planar glass plate and the optical mask. The resulting mixed-scale device could also be used as a master, in which PDMS could be cast against and subsequently used as a polymer stamp to create replicas *via* hot embossing in a single step. Replication of nanoslits in the thermoplastics, PMMA, cyclic olefin copolymer, COC, and polycarbonate, PC, using both methods will be presented.

The major challenge associated with nanofluidic *via* formation in thermoplastics is the enclosure of the channels using thermal fusion bonding with a temperature above the substrate's and covers plate's T_g, which can result in nanostructure collapse and thus, device failure. In this work, we used oxygen plasma treatment of both the cover plate and substrate that resulted in lowering the T_g of the first few nanometres of the material,[37–39] generating in essence a surface confined glue that allowed assembling the device below the T_g of the bulk material. Characterization of imprinted nanostructures in polymers after thermal assembly will be reported. As an example of the utility of these thermoplastic devices for biological applications, dsDNAs were translocated through the nanofluidic slits and the degree of stretching of appropriately stained dsDNAs (λ-DNA) was determined. The translocations were carried out using both COC and PMMA devices to determine if any potential material dependent behavior on the translocation process could be observed.

Experimental

Fabrication of the micromolding and nanoimprinting tools

The micromolding tool was fabricated according to the procedures described by our group.[40] A brief description of the process is provided here. The design of the microstructures was prepared using AutoCAD (Autodesk Inc., San Rafael, CA). The design contained a 4 × 5 array of microstructure patterns with each pattern forming a single device. Each device was composed of two U-shaped microchannels with a minimum separation distance of 60 μm; this distance set the nanoslit length after imprinting. The microchannels were 60 μm wide and 90 μm deep. Each channel had two fluid reservoirs (1.0 mm diameter), one at each of its two termini. The microstructures were milled into a brass template (0.25 inch thick alloy 353 engravers brass, McMaster-Carr, Atlanta, GA) using a high-precision micromilling machine (KERN MMP 2522, KERN Micro- and Feinwerktechnik GmbH & Co.KG, Germany). Micromilling of the master was performed with 50 to 500 μm diameter solid-carbide milling bits (McMaster-Carr or Quality Tools, Hammond, LA) at 40 000 rpm.

The nanoimprinting tool was fabricated using standard procedures for producing an optical mask. Briefly, arrays of lines with widths ranging from 2–7 μm and a pitch ranging from 5–20 μm and length of 3.80 mm were designed using AutoCAD (Autodesk Inc.). A pattern generator (GCA Mann 3600, Seattle, WA) was then used to write the design into a square 5″ × 5″ commercial blank photomask substrate (green sodalime, low reflective Cr layer; Nanofilm, Westlake Village, CA). As specified by the manufacturer, the blank photomask was coated with a thin (1000 ± 60 Å) uniform Cr layer and a layer of positive photoresist. Following patterning and development of the exposed resist, the plate was subjected to a Cr etching solution to produce the desired patterns. The thickness of the Cr layer on the glass substrate defined the depth of the nanoslits.

Replication and assembly of mixed-scale fluidic chips

The fluidic network was generated using a two step replication process. In the first step, microchannels were replicated into a 1/16″ thick polymer substrate (PMMA, T_g = 105 °C—Lucite CP; PC, T_g = 150 °C—Lexan, SABIC Polymershapes, New Orleans, LA; COC, T_g = 134 °C—TOPAS 5013L-10, TOPAS Advanced Polymers, Florence, KY) using the brass molding tool and a commercial hot-embossing system (HEX 02, JenOptik Mikrotechnik, Jena, Germany). Prior to imprinting the nanoslits, polymer substrates were baked in an oven at 75 °C overnight to remove any absorbed moisture. Hot embossing of microchannels was performed at a temperature of 160 °C, 1370 kN m^{-2} for

PMMA; 175 °C, 790 kN m^{-2} for COC; and 190 °C, 1370 kN m^{-2} for PC. After embossing, a thin residual polymer film at the backside of the devices was removed using a fly-cutting machine to open feed reservoirs to the microchannels after which individual devices (1.1 × 1.1 cm^2) were cleaned with detergent and rinsed with ultrapure water.

In the next step, the nanoslits were replicated into the polymer substrate using the nanoimprinting tool (Fig. 1a and 2b). The nanoimprinting tool was carefully aligned between the two "U" shaped microchannel networks (Fig. 2a) so that the resulting nanoslits would be perpendicular to the microchannels (see Fig. 1a). The nanoimprinting tool/polymer assembly was then clamped between two glass plates using binder clips and placed into a convection oven. The AFM profile of nanoslits replicated into PMMA is shown in Fig. 2c. Imprinting conditions were optimized to achieve high replication fidelity into the polymer and at the same time minimize deformation in the microchannels (see ESI, Fig. S1†). Patterning of nanostructures into the thermoplastics utilized the following conditions: PMMA—110 °C, 160 kN m^{-2} for 10 min; COC—130 °C, 160 kN m^{-2} for 10 min; and PC—147 °C, 370 kN m^{-2} for 10 min.

The second replication process consisted of a single embossing step and used a polymer stamp made from PDMS. A PDMS base and curing agents (Dow Corning Corporation, Midland, USA) were mixed at a ratio of 10 : 1 (w/w) to obtain a PDMS prepolymer solution. The solution was degassed under vacuum for 30 min and then poured on top of the PMMA replicated micro- and nanostructures then degassed again under vacuum. The cast PDMS was then cured in an oven at 85 °C for 4 h. The resulting PDMS stamp containing both the microstructures and nanostructures was peeled from the PMMA master, positioned over a blank PMMA substrate and clamped between two glass plates. Two copper blocks were used as spacers to achieve a final thickness of the PMMA replica of ~1 mm.[41] Embossing of PMMA parts using the PDMS stamp was carried out at 155 °C and a pressure of 160 kN m^{-2} for 30 min.

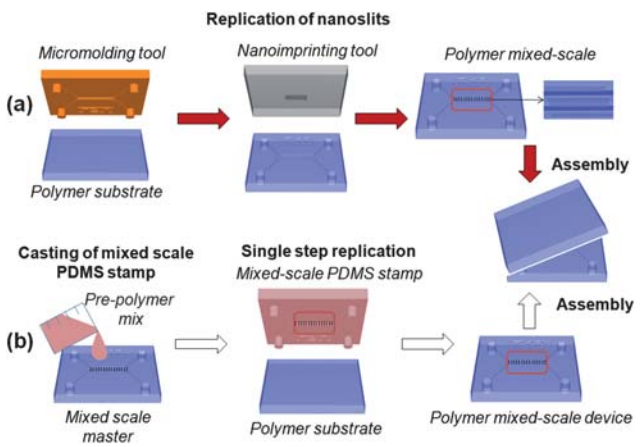

Fig. 1 Step-by-step schematic of the replication processes used to produce polymer mixed-scale polymer devices. (a) Two-step replication process of mixed-scale polymer device using a precision milled micromolding tool and an optical mask as the nanoimprinting tool. (b) Single-step replication for direct hot embossing of the mixed-scale structures using a PDMS elastomeric stamp.

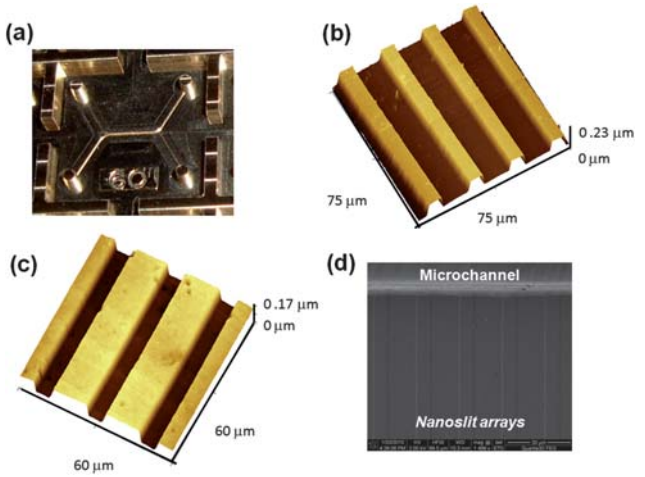

Fig. 2 (a) Photograph of the brass multi-level micromolding tool. (b) AFM 3D-profile of the nanoimprint tool to produce nanoslit arrays; 114 (±4) nm in height with a width of 7 μm and a pitch of 12 μm. (c) AFM 3D-profile of the imprinted nanoslits in PMMA, which were 110 nm in depth, 7 μm in width with a pitch of 12 μm. (d) SEM of a replicated PMMA device showing the micro- and nanofluidic elements.

The mixed-scale structures were enclosed with a thin polymer film consisting of a material similar to that of the substrate using thermal fusion bonding (125 μm thick PMMA, GoodFellow, Oakdale, PA; 110 μm thick COC, TOPAS 5013, TOPAS Advanced Polymers; 125 μm thick PC, SABIC Polymershapes). Thermal fusion bonding was performed using either unmodified polymers or immediate after treating both the cover plate and substrate with an oxygen plasma for 3 min at 18 W (PDC-3XG Plasma Cleaner, Harrick Scientific Products, Pleasantville, NY). The substrate and cover plate were clamped between two glass plates using binder clips and subjected to the optimized thermal fusion bonding protocol. The conditions for cover plate attachment for each polymer material are shown in Table 1.

Metrology and surface characterization

An atomic force microscope (AFM, Model 5500, Agilent Technologies, Santa Clara, CA) was used in tapping mode for

Table 1 Summary of chip assembly conditions and bonding strengths of assembled mixed-scale polymer devices. The numbers in parenthesis represent the standard deviation ($n = 3$).

	PMMA		COC		PC	
Parameters	Native	Oxygen plasma	Native	Oxygen plasma	Native	Oxygen plasma
Bonding temperature/ °C	107	87	130	115	149	130
Bonding pressure/ kN m^{-2}	160	160	160	370	370	370
Bonding time/min	30	30	30	30	30	30
Tensile strength/N cm^{-2}	17 (±3)	2.0 (±0.8)	89 (±5)	14 (±2)	99 (±8)	18 (±3)

determining nanoslit topology and surface roughness. Non-contact AFM tips (PPP-NCL) were obtained from NanoMore (SC, USA). The AFM data were analyzed using freeware Gwyddion software version 2.13 (http://gwyddion.net).

Tensile measurements (MTS Insight® Electromechanical Testing Systems, Eden Prairie, MN) were used to evaluate the bond strength between the substrate and the cover plate. The bond strengths were recorded for devices assembled using plasma treatment with low temperature bonding or thermal fusion bonding at the T_g of the substrate and cover plate without plasma treatment (see Table 1 for chip assembly conditions). Epoxy glue was used to carefully mount two aluminium blocks onto the substrate and cover plate of the assembled fluidic device. After curing, the entire set-up was loaded directly into the tensile machine sample holder for performing the measurement. The measurements were performed using a 5000 N load cell, 50.8 mm grip separation, test speed set to 0.5 mm min^{-1} and a data acquisition rate of 500 Hz.

Chemical compositions of the polymer surfaces were evaluated using X-ray Photoelectron Spectroscopy, XPS (AXIS 165 High Performance Multi-Technique Surface Analysis, Kratos Analytical/Shimadzu Group Company, Columbia, MD). XPS data were acquired using an AlKα source and a hemispherical electron energy analyzer.[30] The pressure in the analyzing chamber was $<3 \times 10^{-9}$ Torr. Survey spectra were recorded with 80 eV pass energy and a 150 W X-ray beam. High-resolution elemental spectra were recorded with 40 eV pass energy and a 150 W X-ray beam. The normal emission angle integrated, high resolution scans with 15–20 eV windows were acquired for the C1s and O1s regions. The reported binding energies were based on the analyzer energy calibration of the Au 4f peak measured at 84.0 eV.

DNA translocation and imaging

Tris–acetate and EDTA buffer (1 × TAE), 40.0 mM, was prepared using 10 × TAE, pH 8.30, stock buffer (Sigma, Saint Louis, MO) and ultrapure water (NANOpure Infinity System, Barnstead, Dubuque, IA). β-Mercaptoethanol (4% v/v) was added into the buffer to minimize photobleaching of the fluorescent staining dye. A bis-intercalating fluorescent dye, YOYO-1® iodide (491 nm/509 nm), was purchased from Molecular Probes (Eugene, OR) and λ-DNA (48.5 kbp) was secured from New England BioLabs (Ipswich, MA). YOYO-1® iodide solutions were prepared in 1 × TAE buffer containing β-mercaptoethanol (4% v/v). The stained dsDNA was prepared fresh prior to the translocation experiments by adding a 5 : 1 molar ratio (bp/dye) of the YOYO-1® dye, λ-DNA and β-mercaptoethanol (4% v/v) and incubated for 2 h at room temperature. All reagents were filtered using a 0.2 μm filter and degassed with an ultrasonicator prior to use. A fluorescein solution (0.5 mM, Sigma, St Louis, MO) was either electrokinetically or vacuum driven through the nanoslits to evaluate nanoslit integrity and sealing.

The high-voltage (HV) power supply used for the translocation experiments was built in-house and consisted of four independent HV modules (EMCO, Sutter Creek, CA, USA). The HV power supplies and relays were controlled by a computer using an analog output card (PCI-DDA04/12, National Instruments, Austin, TX, USA). The controlling software was written in LabView (National Instruments).

All fluidic vias were rinsed with a series of solutions prior to the DNA translocation experiments. First, a binary mixture of methanol/ultrapure water (50% v/v) was introduced into the fluidic conduits. Next, the chip and reservoirs were filled with ultrapure water to rinse the previous solution from the fluidic network. This was followed by adding the appropriate buffer solution to the chip (1 × TAE with 4% β-mercaptoethanol). Each rinsing step was done for approximately 5 to 10 min. Prior to the translocation experiment, the buffer solution in one of the microchannels was replaced with a buffered solution containing the stained dsDNA.

The individual stained λ-DNA molecules were monitored with an inverted microscope (Axiovert 200 M, Carl Zeiss, Thornwood, NY), which was equipped with a 100×/0.93 NA oil immersion objective (Carl Zeiss) and illuminated by a Xe arc lamp. A filter set (λ_{ex} 450–490 nm, λ_{em} 515–565 nm, Carl Zeiss) was used for fluorescence imaging. Images were acquired using an electron multiplying CCD (EMCCD, PhontonMax 512B, Princeton Instruments, Trenton, NJ) at a rate of 20 Hz. Individual frames were extracted from the videos using Winspec 32 software (Princeton Instruments, Trenton, NJ).

Results and discussion

Fabrication of mixed-scale micro-/nanofluidic networks

The fabrication process that was used to make micro- and nanofluidic networks in thermoplastics is shown schematically in Fig. 1. In Fig. 1a, a two-step replication route is described. The first replication step used a metal molding tool to hot emboss microfluidic channels into a thermoplastic substrate. This molding tool consisted of two levels and was fabricated by HPMM (Fig. 2a).[40] The two-level molding tool permitted the fabrication of both the microfluidic channels and fluidic reservoirs in a single replication step eliminating the need for drilling the reservoirs after embossing the microfluidic network, therefore avoiding residual rough edges around the reservoirs. In the second step, nanoslits were produced using nanoimprinting to pattern these structures onto the substrate already containing the microchannels (see Fig. 1a). A commercial optical mask patterned photolithographically was used as the nanomolding tool. The thickness of the Cr layer determined the depth of the nanoslits whereas the lateral dimension was defined by optical lithography.

It was critical for this two-step process that the second replication step did not lead to deformation of the structures formed during the first step. The amount of polymer flow during imprinting is dependent on the imprinting temperature (T_I), the applied imprinting pressure (P_I), and the time used during processing. Hot embossing of microfluidic structures is typically done at a temperature 30–50 °C higher than the T_g of the polymer and pressures of ~500 to 20 000 kN m^{-2}.[40,42–45] The combination of relatively high temperatures and pressures ensures that the polymer can flow easily into the molding tool resulting in high fidelity replication of microstructures with low residual stress in a reasonably short time period (1–5 min). In general, the polymer substrate flows over a distance that depends

on the width and depth of the raised structure in the mold.[46] For microchannel hot embossing, the polymer has to flow over tens of micrometres, whereas for nanoslit replication, only minimal bulk flow of the polymer is required due to the shallow depth of the protrusions. We successfully replicated nanoslit patterns into different thermoplastic polymers using our nanomolding tool. Fig. 2d presents an SEM of microchannels and nanoslits replicated using this two-step process. The amount of microchannel deformation, defined as the change in the cross-sectional area before and after nanoimprinting, was characterized at various nanoimprinting conditions. It was determined that microchannel deformation could be kept to less than 5% when optimized imprint conditions were used without scarifying the quality of the imprinted nanoslits as well (see Fig. S1 in the ESI†). The optimized conditions were as follows: PMMA—P_I = 160 kN m^{-2} and T_I = 110 °C; COC—P_I = 160 kN m^{-2} and T_I = 130 °C; PC—P_I = 370 kN m^{-2} and T_I = 147 °C.

The major advantage of the two step approach is the flexibility it affords for fabricating the micromolding and nanoimprinting tools. For example, different techniques can be used for the micromolding tool such as LiGA, HPMM, laser ablation, electrical discharge machining, dry/wet etching, or lithography.[24] In a similar fashion, there are multiple routes to fabricate the nanoimprinting tool, such as focused ion beam milling[47] or electron-beam lithography followed by wet/dry etching.[20,48] Given that the two-step replication process decouples the nanoimprinting from the micromolding step, one can mix-and-match different mold preparation techniques as well as the molding conditions depending on the specifications of the final product and available resources.

Alternatively, the patterned substrate can also be used as a master for the fabrication of a mixed-scale polymer stamp, which can then be used for single step replication of mixed-scale structures as shown in Fig. 1b. Various polymers have already been demonstrated as viable molding stamps for hot embossing of thermoplastics including PDMS, polyether ether ketone, polysulfone, polyimide, photoresists such as SU-8 and other UV curable epoxies.[49–52] An important requirement is that the polymer used as the molding stamp remains structurally stable at temperatures above the T_g of the polymer being patterned. PDMS has been shown to be a viable stamp material for replicating thermoplastic devices.[48,49,51,52] PDMS possesses excellent replication properties, it can be easily cast against a mold master and cured with minimal shrinkage, thus generating good replication fidelity.[48] In addition, cured PDMS is stable at temperatures exceeding 200 °C, which is higher than the T_g of many thermoplastics such as PMMA, PC, and COC.

To demonstrate this concept, we used a PMMA substrate patterned with mixed-scale structures as the master for casting PDMS to generate a transfer molding stamp. An SEM image of the PDMS stamp is depicted in Fig. 3a. The PDMS molding stamp was used to transfer mixed-scale fluidic structures into PMMA sheets using a single hot embossing step (see Fig. 1b). We were able to successfully replicate both micro- and nanostructures into the PMMA using hot embossing and the PDMS stamp, although some geometrical deformation of the embossed structures compared to the PDMS stamp were observed. For example, the depth of the embossed PMMA nanoslits was measured to be ~70% of the corresponding structure of the

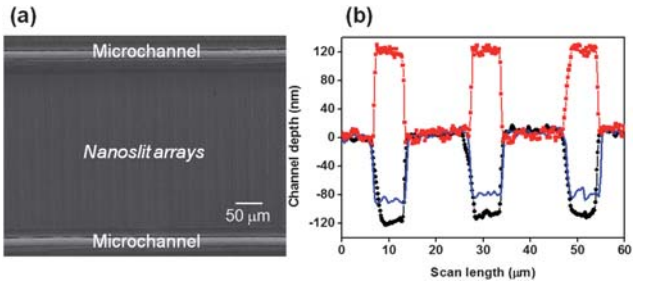

Fig. 3 (a) SEM image of the mixed-scale PDMS stamp. (b) AFM profiles of the PMMA master (black-circle line); PDMS stamp (red-square line); and the PMMA embossed nanoslits (blue solid line).

PDMS stamp (Fig. 3). Results of both nano- and microembossing using PDMS stamps reported previously demonstrated near 100% replication fidelity. For example, long embossing cycle times and the use of vacuum have been identified as parameters requiring optimization for producing high fidelity replicates using elastomeric stamps.[49] Harder PDMS formulations (*i.e.*, 5 : 1 ratio of the elastomer precursor and curing agent mixture rather than the standard 10 : 1 ratio) increase the modulus of elasticity of PDMS leading to higher replication fidelity as well.[49] Alternatively, other polymer materials used for the transfer molding stamp, such as a UV-curable resins, can potentially improve the replication fidelity.[52] We are currently working on improving the nano-stamping fidelity by testing many of the aforementioned parameters.

Our preliminary experiments indicate that the stamp can be used for >5 cycles based on AFM profile traces of the stamp (data not shown). PDMS stamp lifetime is predominantly dependent on the aspect ratio of its structures.[49] Our PDMS stamp contained mixed-scale structures (microchannels—60 μm width and 90 μm depth; nanoslits—7 μm width, 100 nm depth) and thus, the aspect ratio (AR) was 1.5 for the microchannels and ~0.01 for the nanoslits. However, it has been reported that PDMS molding tools can be successfully used for ~20 cycles for hot embossing microchannels (AR ≈ 2; 5–250 μm depths; >40 μm width).[49]

Chip assembly

Following replication of the micro- and nanostructures using top-down approaches, the replicated conduits must be enclosed with a cover plate for fluidic operation. A common method used to enclose fluidic networks on the micrometre-scale is thermal fusion bonding a cover plate to the replicated substrate. During this process, the cover plate and substrate are brought into conformal contact and heated above their T_g at which point, materials fuse together due to the mobility afforded by the polymer when heated above its T_g. By careful control of the temperature, pressure, and time, a strong bond between the materials with minimal structural deformation can be achieved.[53,54] However, thermal fusion bonding of polymer-based devices patterned with nanostructures is more challenging due to the bulk flow and deformation of the polymer under pressure and temperatures approaching the T_g. For example, it has been demonstrated that thermal fusion bonding can lead to a 0.7 μm

change in the depth of a microchannel.[54] This constitutes only a 2% change for a channel depth of 37 μm, however, it would cause complete loss of structural integrity for nanostructures (~100 nm).[54]

To avoid problems with nanoslit collapse or deformation during thermal fusion bonding at or slightly above the T_g of the substrate, different surface treatments can be used, such as oxygen plasma, UV, or UV/O_3, which have been proposed for thermal fusion bonding.[39,55,56] It is well documented that these protocols introduce oxygen rich moieties, such as hydroxyl, carbonyl, and carboxyl groups, onto the surface of the polymer through different free-radical reactions and effectively increase the hydrophilic character and reduce the surface energy of the polymer.[28,31] These protocols can also produce a thin layer of polymer with much shorter chains (lower molecular weight) through chain scission induced by the perturbing radiation. This layer is characterized by a lower T_g compared to the bulk and as such can work as a reactive layer leading to the ability to bond polymer chips below the T_g of the bulk material preventing surface reorganization or structural deformation of the replicated structures.

In the present work, we employed an oxygen plasma treatment of the polymer surfaces to achieve successful thermal fusion bonding of substrates to cover plates below the bulk T_g to minimize any nanostructure deformation and/or collapse during assembly. For the thermal fusion bonding following oxygen plasma treatment for chip assembly, we used 87 °C for PMMA, 115 °C for COC and 130 °C for PC. No bonding between the cover plate and the embossed substrates was observed at the aforementioned temperatures without oxygen plasma treatment (data not shown). In order to assess possible nanostructure deformation due to the thermal fusion bonding process, we evaluated cross-sectional profiles of the nanoslits before and after subjecting them to the thermal fusion bonding process. Fig. 4a and b show AFM profiles of nanoslits replicated in PMMA and COC, respectively. To make the channels accessible to the AFM tip following thermal fusion bonding, the cover plate was carefully removed from the chip without damaging or cracking the substrate. As can be observed from these profiles, substrates subjected to oxygen plasma treatment and low temperature bonding (Fig. 4a and b) showed ~6% (PMMA) and 9% (COC) reduction in the depth of the slit compared to the nanoslits without chip assembly, but there was no observed reduction in the width of the structures (see Fig. 4a and b). On the other hand, nanoslits that were not subjected to oxygen plasma treatment and thermal bonding close to the bulk T_g of the material (107 °C for PMMA and 130 °C for COC) collapsed by 40% and 60% for PMMA and COC, respectively. The reduction in structure height could be due to material deformation following thermal fusion bonding and/or partial loss of material from the nanoslit substrate or cover plate following removal of the cover plate from the substrate. As can be seen in the AFM profile for the PMMA nanoslits for the condition of thermal bonding close to the bulk T_g (blue-dashed line in Fig. 4a), the surface roughness was significantly greater than this same surface prior to chip assembly. This could indicate material was either added to or removed from the substrate or cover plate following cover plate removal. Interestingly, this was not observed in the case of the COC nanoslit device (blue-dashed line in Fig. 4b). Potential material loss from the substrate when subjected to oxygen plasma treatment and low temperature thermal fusion bonding would not be expected because the bonding strength between the substrate and cover plate was significantly lower (see Table 1). Indeed, AFM data supported this supposition (data not shown).

It was also observed that nanoslit collapse was accompanied by collapse of the cover plate as well as making the nanoslits unusable for fluidic testing when bonding was accomplished close to the bulk T_g of the material. However, even in the case of bonding below the T_g for the bulk substrate following plasma activation of the material, we observed slight cover plate collapse (see Fig. S2 in the ESI†).

Evaluation of thermal fusion bonding strength

Tensile measurements were used to measure the bond strength between the patterned substrate and the cover plate following different bonding protocols. The results are summarized in Table 1 along with the specific thermal fusion bonding conditions used. The bond strengths recorded for the plasma-treated polymers when bonded below the bulk substrates' T_g were 2.0 ± 0.8 N cm^{-2} for PMMA, 14.1 ± 1.7 N cm^{-2} for COC, and 18.1 ± 2.7 N cm^{-2} for PC. As a reference, we also evaluated thermal fusion bonding at or above the bulk T_g, because this condition is typically applied for thermal fusion bonding of microchips even though this leads to nanoslit collapse. These bond strengths were: 17.5 ± 3.5 N cm^{-2} for PMMA, 88.8 ± 5.0 N cm^{-2} for COC and 99.8 ± 8.0 N cm^{-2} for PC. It is clear that the bond strengths obtained for the oxygen plasma treated polymers with thermal fusion bonding below the T_g of the bulk material were lower than those bonded at a temperature greater than the bulk T_g and not subjected to the oxygen plasma. Because polymer fusion is limited to the plasma treated surface layer only, lower bonding strengths were expected when compared to bonding at the bulk T_g, where bulk polymer flow takes place. Even though the bonding strength for the oxygen plasma treated material was lower, there was no noticeable disassembly or leakage of the device when flowing fluorescent dye solutions through these nanoslits. The yield of successful chip assemblies using our optimized protocol was ~90%.

The quality of the seal between the cover plate and imprinted substrate was also tested by filling the channels with a solution of a fluorescent dye and imaging the emission using a fluorescence microscope. Fluorescence images of the polymer nanoslit arrays (~100 nm) filled with fluorescein are shown in Fig. 4c and d for 7 μm wide and 2 μm wide nanoslits, respectively. It is clear that no leakage between adjacent nanoslits was observed as the fluorescent signal was confined to the nanopatterned area only.

Surface roughness

The surface roughness of nanoslits imprinted into PMMA and COC was investigated using AFM after chip surface treatment and thermal fusion assembly. Prior to AFM interrogation, the cover plate was removed from the assembled chip without causing damage to the nano-imprinted substrate. The root-mean-square (RMS) roughness of the imprinted PMMA

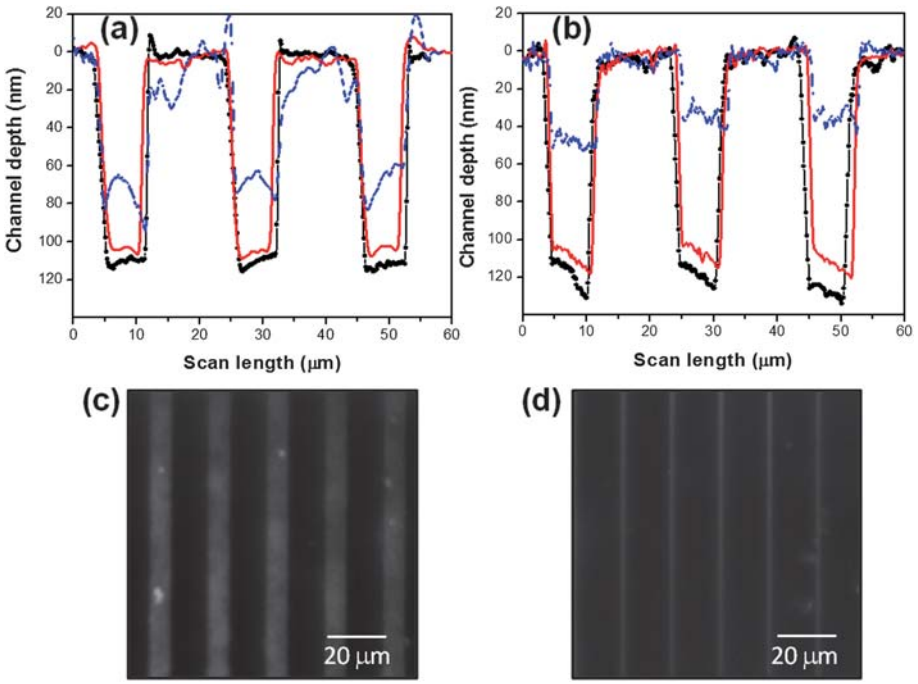

Fig. 4 AFM profiles measured for (a) PMMA and (b) COC nanoslits before and after different cover plate assembly protocols. Also shown are fluorescence images of the nanoslit array (~100 nm deep) filled with 0.5 mM fluorescein solution in TAE 40.0 mM buffer at pH 8.3 for: (c) PMMA nanoslits (7 μm wide, 12 μm pitch) and (d) COC nanoslits (2 μm wide, 18 μm pitch). The blue-dashed line represents the slit depth following thermal fusion bonding at 107 °C for PMMA and at 130 °C for COC slits; red solid line is the depth of the slits following thermal fusion bonding at 87 °C and 115 °C of oxygen plasma treated substrate and cover plate for PMMA and COC, respectively; and the black-circle line is the nanoslits following molding, but not subjected to thermal fusion bonding.

nanoslits was 6.8 ± 0.5 nm, whereas the RMS roughness for the COC nanoslits was 6.0 ± 1.0 nm, which was slightly lower than that obtained from PMMA. The RMS roughness of the nano-molding tool was found to be 0.8 ± 0.1 nm (see Fig. 2b). In general, RMS roughness of molding tools should be similar to the roughness produced in the molded substrate. We suspect that sticking between the molded polymer and imprinting tool caused an increase in this roughness. In addition, the higher RMS roughness could have resulted from the oxygen plasma treatment.[31] Work is currently on-going to reduce this roughness.

XPS surface analysis of nanoimprinted polymer substrate

Chemical compositions of the imprinted polymer surfaces were evaluated using X-ray Photoelectron Spectroscopy, XPS. The O1s/C1s ratio for all three polymers (PMMA, COC, and PC) increased after oxygen plasma treatment, confirming the introduction of oxygen containing functional groups (see Table S1 and Fig. S3†). These results are in agreement with the observed decrease in the water contact angles of the polymers following plasma treatment. The water contact angles of PMMA, COC and PC decreased by 15%, 75%, and 52%, respectively, following oxygen plasma treatment (PMMA–Native 67 ± 2°, PMMA–O_2 plasma 57 ± 2°; COC–Native, 92 ± 2°, COC–O_2 plasma 23 ± 2°; PC–Native 82 ± 1°, and PC–O_2 plasma 39 ± 3°). Introduction of oxygen-containing groups to the polymer surface is beneficial as it increases the wettability/hydrophilicity of the polymer surface, which facilitates filling the nanoslits with aqueous solutions.

Translocation of λ-DNA through thermoplastic nanoslits

We were interested in evaluating the utility of the thermoplastic-based nanoslits for DNA extension, which could find important applications in sizing or mapping dsDNAs for diagnostic applications. In addition, we evaluated whether different substrate materials may affect the performance of the device for dsDNA stretching. Therefore, λ-DNA stretching inside PMMA and COC nanoslits was carried out. The λ-DNA was fluorescently stained with the bis-intercalating dye, YOYO-1®, and transported through the slits electrokinetically. Fig. 5a shows the DNA mobility *vs.* the applied electrical field strength for both polymeric materials. The apparent DNA mobilities were calculated using the expression, $\mu_{a_{DNA}} = (l/tE)$, where $\mu_{a_{DNA}}$ is the measured DNA apparent mobility in the presence of EOF, l is the nanoslit length (60 μm), t is the DNA translocation time (s) through the nanoslit and E is the electrical field strength (V cm^{-1}). Electric field strengths in the nanoslits were calculated based on the fact that the majority of the circuit resistance is through the nanoslit region, allowing the calculation of the total voltage drop across the nanoslit.[57] Fluorescence images of λ-DNA translocation through the nanoslits are presented in Fig. 5b and c for COC and PMMA nanoslits.

It can be seen that at similar electric field strengths, the DNA molecules tend to accumulate at the inlet and outlet ends of the nanoslits (see Fig. 5b for outlet end of COC nanoslits and Fig. 5c for inlet end of PMMA nanoslits). This may be due to extensive surface roughness of the microchannel walls when replicated from the brass molding tool, which has much higher surface roughness (~115 nm)[40] compared to the nanoslit surface

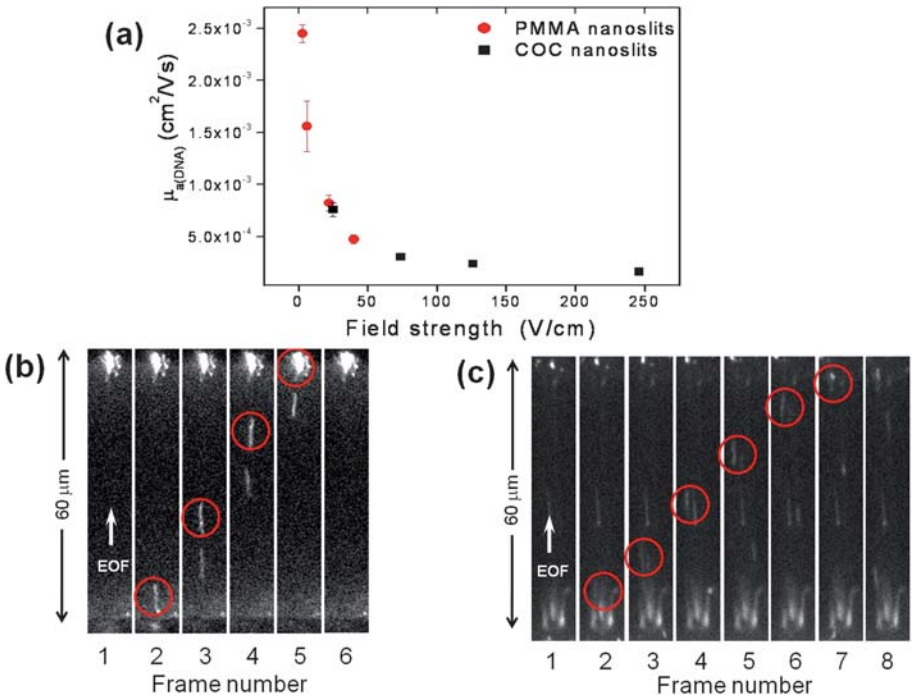

Fig. 5 (a) Plots of DNA mobility *vs.* electric field strength for PMMA and COC mixed-scale fluidic devices. The nanoslit dimensions were ~100 nm deep and 7 μm wide. Error bars represent the standard deviations in the measurements ($n = 3$). Fluorescence images of λ-DNA-YOYO®-1 translocation through nanoslits in (b) COC and (c) PMMA devices.

roughness (see Fig. 2c). It has been reported that along the surface of relatively rough channels, dielectrophoretic trapping can result from non-uniform electrical field gradients.[11,16,58]

In our DNA translocation experiments, we were able to observe DNA movement through the slits without utilizing an EOF suppressor. EOF suppression is typically required for fused silica-based devices.[59] The EOF in COC has been reported to be 3.7×10^{-4} cm^2 V^{-1} s^{-1} and this is slightly higher than that for PMMA (3.3×10^{-4} cm^2 V^{-1} s^{-1}), but both are substantially lower than the EOF observed for glass or fused silica.[22,60]

DNA mobilities were next calculated at a similar field strength (~25 V cm^{-1}) and these were found to be $8.23 \pm 0.74 \times 10^{-4}$ cm^2 V^{-1} s^{-1} and $7.62 \pm 0.65 \times 10^{-4}$ cm^2 V^{-1} s^{-1} for PMMA and COC, respectively. Fig. 5a shows decreases in the apparent mobility with increasing electric field strength for both PMMA and COC nanoslits. Intermittent stationary behavior of DNA in both PMMA and COC nanoslits was observed even in the presence of an electric field. Fig. S4a and S4b (see ESI†) show the intermittent stationary behavior of dsDNA molecules inside COC nanoslits.

λ-DNA (48.5 kbp) has a contour length of 16.2 μm and when stained with an intercalating dye such as YOYO-1® at the concentration employed here, the contour length is increased to 18.6 μm.[61] Extension lengths of dsDNA were measured in PMMA and COC nanoslits from the fluorescence image captured during the DNA translocation. The extension factor was calculated using, $\varepsilon = (L_z/L)$, where ε is the extension factor, L is the full contour length (18.6 μm), and L_z is the measured extension length (μm).[12] The extension length, L_z (μm), in the regime where the channel size is greater than the biopolymer persistence length (~50 nm), as in the present case, can be estimated from the de Gennes theory with the degree of stretching dependent upon the channel size, persistence length of the molecule and the width of the molecule.[62] The extension factors for λ-DNA in this work were found to be 0.46 for PMMA and 0.53 for COC nanoslits (standard deviation 2–6%, $n = 4$). While the slit dimensions were similar in both cases, we did note differences in the extension factors obtained for COC and PMMA that would not be predicted based solely on the de Gennes theory.[62] The degree of extension may also depend on surface energies; oxygen plasma treated COC surfaces have a lower water contact angle ($23 \pm 2°$) than PMMA ($57 \pm 2°$) and thus different surface energies. Therefore, the physical dimensions of the nano-confined environment may not be the only factor influencing extension, but the material properties of the nano-confined environment as well.

Conclusions

We present herein simple protocols for producing nanoslits in different thermoplastic materials, such as PMMA, COC, PC and others as well. The fabrication processes reported can be applied to different candidate materials with the only modifications required being the embossing/imprinting conditions, such as the temperature and pressure. Two different procedures were described, one used a two-step replication process and in the other a polymer stamp was used to replicate mixed-scale structures in a single step. The two-step fabrication process used a micromolding tool generated by HPMM and an optical mask patterned photolithographically, which served as the nano-imprinting tool. The depth of the nanoslits was determined by the Cr layer thickness; thinner Cr films can be used to produce

shallower slits. The thickness of the Cr layer can be controlled through a variety of deposition processes, such as vacuum deposition, and films with atomic-scale resolution can be successfully generated. Therefore, while 100 nm thick Cr films were used in this study, one can select the nanoslit depth by changing the Cr layer thickness on the glass substrate.

In the second process, the mixed-scale thermoplastic device was used as a master to produce an elastomeric stamp, in this case PDMS, used to replicate polymer parts directly using hot embossing. In both cases, the fluidic architectures were enclosed by assembling a polymer cover plate to the substrate made from the same material. A thermal fusion bonding process was used, which consisted of subjecting the substrate and cover plate to oxygen plasma treatment followed by assembling at a temperature below the bulk material's T_g, which significantly reduced structural deformation. The commonality in both processes is that they are simple and robust and did not require extensive infrastructure and equipment to produce the nanoslits.

Surface roughness of the replicated parts was found to be relatively higher than the molding tool and this was assumed to arise when separating the replicated part manually from the molding tool during demolding and/or oxygen plasma treatment. The addition of surface coatings on the molding tool may alleviate some of these issues and that should improve replication fidelity.

Finally, translocation studies of dsDNA through nanoslits were carried out and as noted in similar studies,[16] field-dependent electrophoretic mobilities were observed due to surface roughness generating inhomogeneous electric fields giving rise to dielectrophoretic trapping.[11,58] Extension factors calculated for the translocating dsDNA indicated potential material-dependent differences. We are currently evaluating different polymeric materials with difference surface energies to understand these effects on dsDNA extension. Also, to significantly improve the degree of extension, the nano-confined environment needs to be scaled well below the persistence length including the lateral dimension, producing nanochannels. Work is underway in our laboratory to generate polymer nanochannels using the replication techniques outlined in this study.

Acknowledgements

This work was supported through funds from the National Institutes of Health (EB-006639), the National Science Foundation (EPS-0346411), and the Louisiana Board of Regents. The World Class University (WCU) program from Ulsan National Institute of Science and Technology (UNIST) is also acknowledged for partial financial support of this work. J. Tamarit-Lopez thanks the Spanish Ministerio de Educacin y Ciencia for his PhD grant. The authors would also like to thank the staff from the Center for Advanced Microstructures and Devices at LSU, especially F. B. Dawan and D. G. Yemane, for assistance with optical mask fabrication and K. Lian for the EMCCD camera utilized throughout this work. Special appreciation to J. Guy for the HPMM of the brass master and J. M. Emory for help with the optical measurements.

References

1 P. Abgrall and N. T. Nguyen, *Anal. Chem.*, 2008, **80**, 2326–2341.
2 J. O. Tegenfeldt, C. Prinz, C. Han, R. L. Huang, R. H. Austin, S. Y. Chou, E. C. Cox and J. C. Sturm, *Anal. Bioanal. Chem.*, 2004, **378**, 1678–1692.
3 N. Douville, D. Huh and S. Takayama, *Anal. Bioanal. Chem.*, 2008, **391**, 2395–2409.
4 J. C. T. Eijkel and A. van den Berg, *Microfluid. Nanofluid.*, 2005, **1**, 249–267.
5 J. Perry and S. Kandlikar, *Microfluid. Nanofluid.*, 2006, **2**, 185–193.
6 H. A. Becerril and A. T. Woolley, *Chem. Soc. Rev.*, 2009, **38**, 329–337.
7 R. Riehn, W. Reisner, J. O. Tegenfeldt, Y. M. Wang, C.-k. Tung, S.-F. Lim, E. Cox, J. C. Sturm, K. Morton, S. Y. Chou and R. H. Austin, in *Integrated Biochips for DNA Analysis*, ed. R. H. Liu and A. P. Lee, Landes Bioscience and Springer Science+Business Media, LLC, Boston, 2007, ch. 12, pp. 151–186.
8 R. Riehn, M. Lu, Y.-M. Wang, S. F. Lim, E. C. Cox and R. H. Austin, *Proc. Natl. Acad. Sci. U. S. A.*, 2005, **102**, 10012–10016.
9 R. Riehn, R. H. Austin and J. C. Sturm, *Nano Lett.*, 2006, **6**, 1973–1976.
10 W. Reisner, K. J. Morton, R. Riehn, Y. M. Wang, Z. Yu, M. Rosen, J. C. Sturm, S. Y. Chou, E. Frey and R. H. Austin, *Phys. Rev. Lett.*, 2005, **94**, 196101.
11 J. Regtmeier, T. T. Duong, R. Eichhorn, D. Anselmetti and A. Ros, *Anal. Chem.*, 2007, **79**, 3925–3932.
12 J. O. Tegenfeldt, C. Prinz, H. Cao, S. Chou, W. W. Reisner, R. Riehn, Y. M. Wang, E. C. Cox, J. C. Sturm, P. Silberzan and R. H. Austin, *Proc. Natl. Acad. Sci. U. S. A.*, 2004, **101**, 10979–10983.
13 S.-m. Park, Y. S. Huh, H. G. Craighead and D. Erickson, *Proc. Natl. Acad. Sci. U. S. A.*, 2009, **106**, 15549–15554.
14 S. Chung, J. H. Lee, M.-W. Moon, J. Han and R. D. Kamm, *Adv. Mater.*, 2008, **20**, 3011–3016.
15 M. Ali, B. Schiedt, R. Neumann and W. Ensinger, *Macromol. Biosci.*, 2010, **10**, 28–32.
16 G. B. Salieb-Beugelaar, J. Teapal, J. van Nieuwkasteele, D. Wijnperle, J. O. Tegenfeldt, F. Lisdat, A. van den Berg and J. C. T. Eijkel, *Nano Lett.*, 2008, **8**, 1785–1790.
17 P. Mao and J. Han, *Lab Chip*, 2005, **5**, 837–844.
18 N. W. Liu, A. Datta, C. Y. Liu and Y. L. Wang, *Appl. Phys. Lett.*, 2003, **82**, 1281–1283.
19 P. E. Shao, A. van Kan, L. P. Wang, K. Ansari, A. A. Bettiol and F. Watt, *Appl. Phys. Lett.*, 2006, **88**, 093515.
20 A. E. Grigorescu and C. W. Hagen, *Nanotechnology*, 2009, **20**, 292001.
21 X. G. Liang, K. J. Morton, R. H. Austin and S. Y. Chou, *Nano Lett.*, 2007, **7**, 3774–3780.
22 H. Shadpour, H. Musyimi, J. Chen and S. A. Soper, *J. Chromatogr., A*, 2006, **1111**, 238–251.
23 H. Becker and L. E. Locascio, *Talanta*, 2002, **56**, 267–287.
24 H. Becker and C. Gärtner, *Electrophoresis*, 2000, **21**, 12–26.
25 C.-W. Tsao and D. L. DeVoe, *Microfluid. Nanofluid.*, 2009, **6**, 1–16.
26 X. G. Liang and S. Y. Chou, *Nano Lett.*, 2008, **8**, 1472–1476.
27 Q. F. Xia, K. J. Morton, R. H. Austin and S. Y. Chou, *Nano Lett.*, 2008, **8**, 3830–3833.
28 S. Wei, B. Vaidya, A. B. Patel, S. A. Soper and R. L. McCarley, *J. Phys. Chem. B*, 2005, **109**, 16988–16996.
29 N. Vourdas, A. Tserepi, A. G. Boudouvis and E. Gogolides, *Microelectron. Eng.*, 2008, **85**, 1124–1127.
30 S. Balamurugan, A. Obubuafo, S. A. Soper, R. L. McCarley and D. A. Spivak, *Langmuir*, 2006, **22**, 6446–6453.
31 J. Chai, F. Lu, B. Li and D. Y. Kwok, *Langmuir*, 2004, **20**, 10919–10927.
32 D. Belder and M. Ludwig, *Electrophoresis*, 2003, **24**, 3595–3606.
33 E. Abad, S. Merino, A. Retolaza and A. Juarros, *Microelectron. Eng.*, 2008, **85**, 818–821.
34 W. Li, J. O. Tegenfeldt, L. Chen, R. H. Austin, S. Y. Chou, P. A. Kohl, J. Krotine and J. C. Sturm, *Nanotechnology*, 2003, **14**, 578–583.
35 L. J. Guo, X. Cheng and C.-F. Chou, *Nano Lett.*, 2004, **4**, 69–73.
36 L. H. Thamdrup, A. Klukowska and A. Kristensen, *Nanotechnology*, 2008, **19**, 125301.
37 P. Kettner, R. L. Pelzer, T. Glinsner and S. Farrens, *J. Phys.: Conf. Ser.*, 2006, **34**, 65–71.
38 P. Abgrall, L.-N. Low and N.-T. Nguyen, *Lab Chip*, 2007, **7**, 520–522.
39 H. Shinohara, J. Mizuno and S. Shoji, *IEEJ Trans. Electr. Electron. Eng.*, 2007, **2**, 301–306.
40 M. L. Hupert, W. J. Guy, S. D. Llopis, H. Shadpour, S. Rani, D. E. Nikitopoulos and S. A. Soper, *Microfluid. Nanofluid.*, 2007, **3**, 1–11.

41 A. P. Russo, D. Apoga, N. Dowell, W. Shain, A. M. P. Turner, H. G. Craighead, H. C. Hoch and J. N. Turner, *Biomed. Microdevices*, 2002, **4**, 277–283.
42 B. Bhushan, *Handbook of Nanotechnology*, Springer, New York, 2007.
43 H. Becker and U. Heim, *Sens. Actuators, A*, 2000, **83**, 130–135.
44 Y.-J. Juang, L. J. Lee and K. W. Koelling, *Polym. Eng. Sci.*, 2002, **42**, 551–566.
45 Y.-J. Juang, L. J. Lee and K. W. Koelling, *Polym. Eng. Sci.*, 2002, **42**, 539–550.
46 C. M. E. Sotomayor Torres, *Alternative Lithography: Unleashing the Potentials of Nanotechnology*, Kluwer Academic/Plenum, New York, 2003.
47 S. W. Youn, C. Okuyama, M. Takahashi and R. Maeda, *J. Mater. Process. Technol.*, 2008, **201**, 548–553.
48 B. D. Gates, Q. Xu, M. Stewart, D. Ryan, C. G. Willson and G. M. Whitesides, *Chem. Rev.*, 2005, **105**, 1171–1196.
49 J. Narasimhan and I. Papautsky, *J. Micromech. Microeng.*, 2004, **14**, 96–103.
50 W. Pfleging, W. Bernauer, T. Hanemann and M. Torge, *Microsyst. Technol.*, 2002, **9**, 67–74.
51 T. L. Edwards, S. K. Mohanty, R. K. Edwards, C. L. Thomas and A. B. Frazier, *Sens. Mater.*, 2002, **14**, 167–178.
52 C. C. Wu and S. L. C. Hsu, *J. Micromech. Microeng.*, 2010, **20**, 015006.
53 J. Greener, W. Li, J. Ren, D. Voicu, V. Pakharenko, T. Tang and E. Kumacheva, *Lab Chip*, 2010, **10**, 522–524.
54 Y. Sun, Y. C. Kwok and N. T. Nguyen, *J. Micromech. Microeng.*, 2006, **16**, 1681–1688.
55 C. W. Tsao, L. Hromada, J. Liu, P. Kumar and D. L. DeVoe, *Lab Chip*, 2007, **7**, 499–505.
56 X. Zhu, G. Liu, Y. Guo and Y. Tian, *Microsyst. Technol.*, 2007, **13**, 403–407.
57 T. Hug, N. Rooij and U. Staufer, *Microfluid. Nanofluid.*, 2006, **2**, 117–124.
58 C.-H. Chuang, Y.-M. Hsu and C.-H. Wei, *Electrophoresis*, 2009, **30**, 3044–3052.
59 J. D. Cross, E. A. Strychalski and H. G. Craighead, *J. Appl. Phys.*, 2007, **102**, 024701.
60 M. Castaño-Álvarez, M. T. Fernández-Abedul and A. Costa-García, *Electrophoresis*, 2005, **26**, 3160–3168.
61 H. Ihmels and D. Otto, in *Topics in Current Chemistry*, ed. F. Würthner, Springer, Heidelberg, 2005, vol. 258, pp. 161–204.
62 P. G. de Gennes, *Scaling Concepts in Polymer Physics*, Cornell University Press, Ithaca, NY, 1979.

